

Surfactant-laden Liquid Thread Breakup Driven by Thermal Fluctuations

Luís H. Carnevale*,¹ Piotr Deuar,¹ Zhizhao Che,² and Panagiotis E. Theodorakis*¹

¹*Institute of Physics, Polish Academy of Sciences, Al. Lotników 32/46, 02-668 Warsaw, Poland*

²*State Key Laboratory of Engines, Tianjin University, 300350 Tianjin, China*

(*Electronic mail: panos@ifpan.edu.pl)

(*Electronic mail: carnevale@ifpan.edu.pl)

(Dated: 20 March 2024)

The breakup of liquid threads into droplets is crucial in various applications such as nanoprinting, nanomanufacturing, and inkjet printing, where a detailed understanding of the thinning neck dynamics allows for a precise droplet control. Here, the role of surfactant in the breakup process is studied by many-body dissipative particle dynamics, in particular the various regime transitions and thread profiles, shedding light on molecular-level intricacies of this process hitherto inaccessible to continuum theory and experiments. Moreover, the role of surfactant in the most unstable perturbation, the formed droplet size, and surfactant distributions have been unraveled. As surfactant concentration rises, both the wavelength and time to breakup steadily increase due to the lowering of surface tension below the critical micelle concentration (CMC) and viscous effects introduced by micelles above the CMC. These changes prior to the breakup lead to larger droplets being formed in cases with higher surfactant concentration. We also compared the thinning dynamics to existing theoretical predictions, revealing that the surfactant-laden breakup starts at the inertial regime and transitions into the thermal fluctuation regime when the concentration is increased. Thus, we illuminate the hitherto poorly investigated and intricate breakup process of surfactant-laden liquid threads driven by thermal fluctuations, contributing to a deeper understanding of this process at molecular scales.

I. INTRODUCTION

The breakup of liquid threads into droplets is a ubiquitous natural phenomenon with diverse applications,¹ such as nanoprinting,² nanoscale manufacturing and chemical processing,³ spraying,⁴ and inkjet printing.⁵ Precise control over droplet size and a comprehensive understanding of the dynamics surrounding the thinning neck, also known as the thinning bridge, near the pinch-off point, is crucial in many of these and other applications.^{6–10} The pinch-off process has been extensively examined in the literature, beginning with the foundational works of Plateau and Rayleigh,^{11,12} who delineated the perturbations leading to the destabilization and subsequent breakup of liquid threads or jets. Emphasizing surface tension’s significance and assuming surface free energy minimization, Plateau established the stability condition, i.e. $1 > 2\pi R_0/\lambda = \chi$, where λ represents the perturbation wavelength, χ signifies the nondimensional wavenumber, and R_0 denotes the initial radius of the undisturbed fluid. Instabilities only arise from perturbations with wavelengths longer than the initial circumference of the liquid thread. Rayleigh, via linear stability analysis of inviscid liquids, derived the growth rate of such perturbations, identifying the wavenumber $\chi = 0.697$ as the point of maximum growth (Rayleigh mode). Expanding on Rayleigh’s work, Weber conducted a similar analysis for viscous fluids, establishing that the characteristic wavenumber, determining the highest growth rate, relies on the ratio between viscous forces, inertia, and surface tension.¹³ This dependence can be expressed through the non-dimensional Ohnesorge number $Oh = \mu/\sqrt{\rho\gamma R_0}$, where μ is the viscosity, ρ density, and γ surface tension.

Given surface tension’s pivotal role in liquid thread breakup, it is unsurprising that numerous industrial applications utilize surfactants to modify fluid properties and enhance process control, particularly in droplet stabilization within emulsions.¹⁴ Surfactants, as amphiphilic molecules, have a hydrophobic and a hydrophilic part. This characteristic leads them to favorably adsorb at the surface of liquids reducing surface tension. However, there exists a maximum surface concentration, Γ_∞ , beyond which the fluid surface cannot accommodate more surfactant. After this point, further increase in the surfactant amount would increase the number of surfactant monomers in the bulk. As a result, these will come together and form aggregates of micellar or other morphologies, depending on the structural characteristics of the surfactant. The minimum bulk surfactant concentration that allows for the formation of these aggregates is known as the critical aggregation concentration (CAC). The more specific term critical micelle concentration (CMC) is also widely

used, but this term rather indicates that these aggregates are actually micelles. Importantly, a fluid with surfactants above the CAC will not experience any more lowering of its surface tension due to the saturation of surfactant concentration at the interface. Hence, any further changes in properties above the CAC can be attributed to a higher concentration and the presence of aggregates in the bulk.

During the thinning process of a liquid thread, surfactants are advected away from the pinching point and, in this case, there is a competition between the advection and the adsorption of surfactants from the bulk toward the interface. If adsorption is much slower than advection, a surface concentration gradient is established that leads to Marangoni stresses that slow down the bridge thinning.¹⁵ Various thinning regimes can occur depending on the balance of forces near the pinch-off. These regimes are typically characterized by the time before breakup $\tau = t_b - t$, where t_b is the time that breakup occurs. When inertial forces dominate (I regime¹⁶), the minimum thread radius at the pinch-off region varies as $h_{min} \sim \tau^{2/3}$. This result was provided by Eggers, who used self-similar theory and the lubrication approximation to simplify the Navier–Stokes equation for an inviscid liquid. He has also shown that a universal regime exists when considering a balance between viscous and inertial forces (VI regime), where $h_{min} \sim \tau$.¹⁶ There is also an intermediate regime where viscous forces are dominant (V regime), which also scales as $h_{min} \sim \tau$ as found by Papageorgiou when analyzing the pinch-off for the Stokes flow.¹⁷ However, in the V regime only viscous and capillary forces are relevant with Re depending on time and reaching infinity as pinch-off is approached. In the VI regime, the inertial forces balance the other forces with Re number going to unity. For this reason, the V regime may be considered as only an intermediate regime, while VI is rather a universal regime from a continuum perspective. Transitions between these regimes may also take place during the thinning process. In particular, Castrejón-Pita et al. have shown the wide range of possible transitions through simulation and experiments.¹⁸ Moreover, when the adsorption of surfactants is much slower than advection, Wee et al. have demonstrated that minimum radius also changes as $h_{min} \sim \tau$, following Papageorgiou’s solution with some corrections to accommodate surface rheological effects.¹⁹ In the opposite limit, when adsorption is much faster, the interface remains at a constant concentration and, instead of a power-law, the thinning dynamics follows an exponential regime where $h_{min} \sim e^\tau$.²⁰ An exponential regime has also been found in the breakup of viscoelastic fluids.²¹

The different regimes discussed so far are only valid until the minimum radius reaches a small enough length scale in which thermal fluctuations become relevant, due to the molecular motion.

This thermocapillary length scale can be defined as $l_T = \sqrt{k_B T / \gamma}$ and depends on the thermal energy $k_B T$, where T is temperature, k_B Boltzmann’s constant, and γ surface tension. Moseler and Landman¹ have studied their influence on the breakup process by applying the lubrication approximation to the Landau–Lifshitz–Navier–Stokes equation, which contains a stochastic stress tensor to model the thermal fluctuations and this model is referred to as the stochastic lubrication equation (SLE). They have found that the surface profile near the pinching point becomes a symmetrical double cone which suppresses the formation of satellite droplets and the model yields predictions comparable to molecular dynamics (MD) simulations. Eggers has demonstrated that in the thermal-fluctuation thinning regime (TF) $h_{min} \sim \tau^{0.418}$ by arguing that surface tension becomes less important in driving the breakup and looking for symmetric self-similar solutions to the SLE.²² This behavior has been confirmed, by Hennequin et al., from experiments using ultralow interfacial tension phases of a colloid-polymer solution.²³ Petit et al. experimentally observed the transition from the VI regime to the TF regime.²⁴

Despite the above studies, much less is known about what is happening when surfactant is present, especially at molecular-level scales. To investigate the behavior of surfactant-laden liquid threads at this small length scale, we use the many-body dissipative particle dynamics method (MDPD).^{25–27} At its core, MDPD employs a coarse-grained representation, grouping particles into clusters to capture the collective behavior of molecular systems through soft-core potential interactions, while at the same time, it can be used to simulate molecular chains, such as surfactants. Combined with the ability to model thermal fluctuations, MDPD allows for a computationally efficient way to simulate systems at scales that are inaccessible to purely macroscopic or atomistic models. Mostly, MDPD and its predecessor dissipative particle dynamics (DPD) have been successful in describing the breakup process for surfactant-free systems. For example, Tiwari et al.^{28,29} have used DPD and observed the symmetric double cone profile shape during pinch-off and were also able to recover the TF regime minimum radius scaling. Mo et al.³⁰ have done a more detailed analysis of the thinning process using DPD and were able to observe the I regime and the TF regime by changing the viscosity and surface tension of the system. They have also shown that the viscosity of a DPD fluid is non-Newtonian and this might affect the power-law exponent of the V regime. Arienti et al.³¹ have revealed that MDPD is also capable of describing the breakup process at different coarse-graining levels and they have also demonstrated the transitions from the I to V regime and then to the TF regime. Zhao et al.³² used MDPD to simulate fluids with different properties and observed different regime transitions when increasing the Oh

number and also have proposed a new final regime that precedes pinch-off, although no explanation on the nature of this regime was given. Moreover, Zhao et al.³³ used both MDPD and SLE to study liquid thread breakup and obtained the same results, however, their TF regime scaling differed from Eggers' solution and this discrepancy was attributed to the neglected influence of surface tension when deriving the power-law. In our previous work,³⁴ we have investigated different systems with MDPD and found that the formation of satellite droplets followed a power-law that depended on Oh and a thermo-capillary number $Th = l_T/R_0$. Despite these studies, we have not been able to find molecular simulations of the breakup process for a surfactant-laden liquid thread. However, different models to simulate systems with surfactant have been used within the MDPD framework. For example, Ghoufi et al.³⁵ proposed one of the first models of a sodium dodecyl sulfate (SDS) molecule via a coarse-grained hydrophilic and three hydrophobic particles, where parametrization of intermolecular interactions is based on the Flory–Huggins theory. In another study, Zhou et al.³⁶ modeled SDS and dodecyltrimethylammonium bromide (DTAB) surfactants by first matching the surface tension of each particle to experimental values. Then, the intermolecular interactions were tuned by constructing different multi-component systems. Recently, Hendrikse et al.³⁷ proposed a different parametrization scheme to model alkyl ethoxylate surfactants. In this case, they first match the surface tension and density of each particle to experimental values at a given coarse-grained level and the cross-interactions were obtained from the activity coefficients at infinite dilution computed from the excess chemical potential.

In view of the insufficient fundamental understanding of the breakup process in the presence of surfactant at a molecular scale, we have undertaken the task of exploring this phenomenon in depth by investigating various key properties. Specifically, we have carried out MDPD simulations of threads that are long enough to examine how the surfactant concentration changes the characteristic wavenumber that identifies the perturbation with the highest growth rate leading to breakup. In addition, we check the difference in sizes of main droplets and satellite droplets formed after the breakup for each case considered, and also the minimum radius thinning dynamics was investigated and compared with scaling laws of the aforementioned regimes. Lastly, we present the different thread profiles near pinch-off along with the surfactant distribution on the surface and in the bulk phase, elucidating the surfactant transport mechanism as the system evolves towards breakup. Through this thorough investigation, we aim to shed light on the nuanced molecular mechanisms underpinning this phenomenon, thereby contributing to a more comprehensive un-

derstanding of surfactant-laden breakup processes at the molecular scale. This will offer further possibilities in tailored designs for the relevant applications.

II. MODEL AND METHODOLOGY

A. Many-Body Dissipative Particle Dynamics

The MDPD model is a mesoscale, particle-based model that evolved from its predecessor DPD^{38,39} by adding an attractive and a repulsive contribution between the particles that depends on their local density. This change enables the simulation of systems with liquid–vapor coexistence.^{25,27} MDPD consists in integrating the equation of motion Eq. 1 for every particle i that interacts with the other particles j through a conservative force, \mathbf{F}^C , a random force, \mathbf{F}^R , and a dissipative force, \mathbf{F}^D . The integration of the equation of motion for each particle i is done by using the modified velocity-Verlet algorithm,⁴⁰ where the equation reads

$$m \frac{d\mathbf{v}_i}{dt} = \sum_{j \neq i} \mathbf{F}_{ij}^C + \mathbf{F}_{ij}^R + \mathbf{F}_{ij}^D. \quad (1)$$

The conservative force has a repulsive and an attractive term that act at different lengths. Its most common form is

$$\mathbf{F}_{ij}^C = A \omega^C(r_{ij}) \mathbf{e}_{ij} + B (\bar{\rho}_i + \bar{\rho}_j) \omega^d(r_{ij}) \mathbf{e}_{ij}, \quad (2)$$

where $A < 0$ and $B > 0$ are the attractive and repulsive parameters, respectively, r_{ij} is the distance between particles, \mathbf{e}_{ij} is the direction vector from particle i to particle j , $\omega^C(r_{ij})$ and $\omega^d(r_{ij})$ are linear weight functions defined as follows

$$\omega^C(r_{ij}) = \begin{cases} 1 - \frac{r_{ij}}{r_c}, & r_{ij} \leq r_c \\ 0, & r_{ij} > r_c, \end{cases} \quad (3)$$

$$\omega^d(r_{ij}) = \begin{cases} 1 - \frac{r_{ij}}{r_d}, & r_{ij} \leq r_d \\ 0, & r_{ij} > r_d, \end{cases} \quad (4)$$

with r_c being a cutoff distance for the attractive interaction, usually set to unity, while the repulsive interaction cutoff is usually $r_d = 0.75r_c$. Although not necessary for our purposes, changing r_d affects the parameter space (A, B) where liquid, vapor, and solid phases are present.⁴¹

The many-body contributions in the repulsive force that come from the dependence on local densities $\bar{\rho}_i$ and $\bar{\rho}_j$ are calculated as

$$\bar{\rho}_i = \sum_{j \neq i} \frac{15}{2\pi r_d^3} \left(1 - \frac{r_{ij}}{r_d}\right)^2. \quad (5)$$

Other functions can be used to compute the local densities, such as the kernel functions commonly used in the smoothed particle hydrodynamics (SPH) method.⁴²

To incorporate thermal fluctuations in MDPD, random and dissipative forces are introduced and act as a thermostat, keeping the temperature in the simulation constant and equal to unity. Both can be expressed as

$$\mathbf{F}_{ij}^D = -\sigma \omega^D(r_{ij})(\mathbf{e}_{ij} \cdot \mathbf{v}_{ij})\mathbf{e}_{ij}, \quad (6)$$

$$\mathbf{F}_{ij}^R = \xi \omega^R(r_{ij})\theta_{ij}\Delta t^{-1/2}\mathbf{e}_{ij}, \quad (7)$$

where σ is the dissipative strength, ξ is the strength of the random force, \mathbf{v}_{ij} is the relative velocity between particles, θ_{ij} is a random variable from a Gaussian distribution with zero mean and unit variance. Δt is the timestep, taken to be equal to 0.01. According to the fluctuation–dissipation theorem,⁴³ σ and ξ are related to each other by

$$\sigma = \frac{\xi^2}{2k_B T}, \quad (8)$$

and the weight functions for the forces are

$$\omega^D(r_{ij}) = \left[\omega^R(r_{ij})\right]^2 = \left(1 - \frac{r_{ij}}{r_c}\right)^2. \quad (9)$$

For multi-component systems, $A = A_{ij}$ is the attraction parameter between particles of type i and of type j . The repulsive parameter B has to be the same for all interactions due to the no-go theorem otherwise the force wouldn't be conservative.⁴⁴ Other types of local density functions might be used to circumvent this restriction, however, they have to be carefully defined to avoid unphysical behavior in the simulations.⁴⁵

B. Parametrization

To simulate a physical system with different components in MDPD, it is necessary to define the coarse-graining level, i.e., how many atoms or molecules are represented by one MDPD particle.

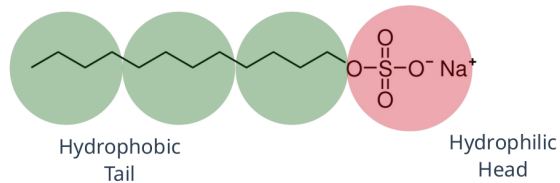


FIG. 1. Schematic representation of the coarse-grained HT_3 surfactant model (see text for details).³⁶

A typical choice is to define one particle as three water molecules and match the model reduced units to real units by measuring some key properties such as density and surface tension for a given set of simulation parameters. In this paper, we have adopted the commonly used values $A_{ww} = -40$ and $B = 25$ (MDPD units), where the subscript ‘w’ denotes the self interaction between water beads, and the dissipative coefficient $\sigma = 4.5$.^{31,46} The conversion between reduced and real units is detailed in Table I. With the interaction between our liquid particles being set, we follow the parametrization of sodium dodecyl sulfate (SDS) surfactant molecules in the same manner as Zhou et al.,³⁶ which was chosen due to its ample use in industrial processes. At the coarse-grained level, the molecule is represented by one ‘H’-type particle, which is the hydrophilic head group of the surfactant and by three ‘T’-type particles, which model the alkane hydrophobic tail of the molecule. Figure 1 shows, schematically, the coarse-grained SDS model.

The self interaction between T particles A_{TT} is tuned to reproduce the surface tension of hexadecane and the cross interaction between w and T particles A_{wT} was adjusted with the interfacial tension between water and hexadecane (T-type particles). The self and cross interactions with the H-type particle were fitted by also measuring the interfacial tension between hexadecane and

TABLE I. Conversion between MDPD units and real units. The scaling is done by matching surface tension and density of water to values measured from MDPD simulations using $A = -40$ and $B = 25$. The coarse-graining level is defined so that one MDPD particle represents three water molecules.

Parameter	MDPD value	Real value
Particle	1	3 H ₂ O
r_c	1	8.17 Å
ρ	6.05	997 kg/m ³
γ	7.62	72 mN/m

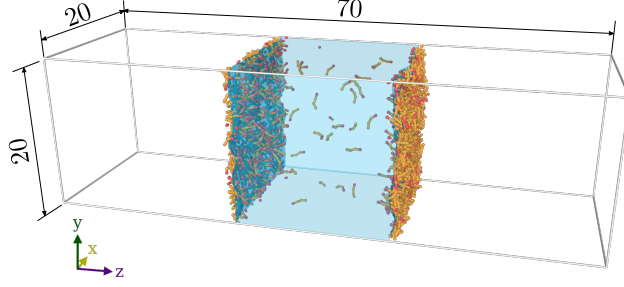


FIG. 2. Example of a simulation box used to measure the surface tension of a liquid slab in the presence of surfactants. The liquid particles are represented by the shaded blue volume for easier visualization. In this case, the concentration of surfactants is below CMC and the surfactant molecules are not aggregated in the bulk phase.

water with SDS molecules at the interface. All interactions are summarized in Table II. Moreover, we used harmonic potentials to model the bonds and angles between particles in the surfactant molecule in order to preserve the structure of the molecule. We found that the bond length and strength proposed by Ref. 36 were not stable in our simulations, so we adopted the values $r_0 = 0.45$, $k = 400$ of Ref. 47, while the same angle potential parameters³⁶ were kept, namely, $\theta_0 = 160^\circ$, $k = 100$.

TABLE II. MDPD interaction parameters for the HT₃ surfactant model and water. W is the water particle, H the hydrophilic particle, and T the hydrophobic particle. The MDPD repulsive parameter is the same for all interactions and is $B = 25$.

A_{ij}	W	H	T
W	-40		
H	-32.18	-19	
T	-27	-5.98	-22

III. RESULTS AND DISCUSSION

A. Surfactant properties

We have conducted a series of simulations to comprehensively characterize the pertinent attributes of our system when surfactants are introduced. The primary focal point of our validation investigation pertains to the surface tension, specifically its change by varying surfactant concentration. Figure 2 shows the standard setup used in simulation to measure the surface tension based on the Kirkwood–Buff method.⁴⁸ Since the CMC is reached when the interface is saturated, the initial surfactant concentration can be defined as the total number of surfactant molecules N_t divided by the initial surface area of the system A_s , namely, $C = N_t/A_s$, while the surface excess concentration is obtained by counting only the number of molecules on the surface divided by the surface area, $\Gamma = N_s/A_s$. Lastly, bulk concentrations are also presented in terms of the surface area $C_b = N_b/A_s$, and, therefore, $N_t = N_b + N_s$. Our simulations for determining the surface tension

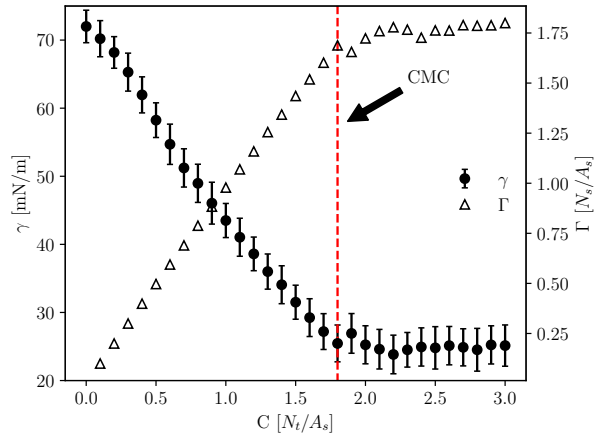


FIG. 3. Dependence of surface tension, γ (circles) and surface excess concentration, Γ (triangles), on the number of surfactant molecules per surface area, C . Both values reach a plateau after crossing the CMC (dashed line) indicating that the interface is fully saturated.

for the water–SDS–surfactant system start with the initialization of a water slab with a thickness $h = 20$ and particle number density $\rho = 6.05$ at the midpoint of the periodic simulation box. This box was defined by dimensions of $L_x = L_y = 20$ and $L_z = 70$ (Figure 2). Subsequently, surfactant molecules were positioned directly at the interfaces of this water slab, and we allowed the system to run 10^5 time steps to attain thermodynamic equilibrium. Once equilibrium was reached, we

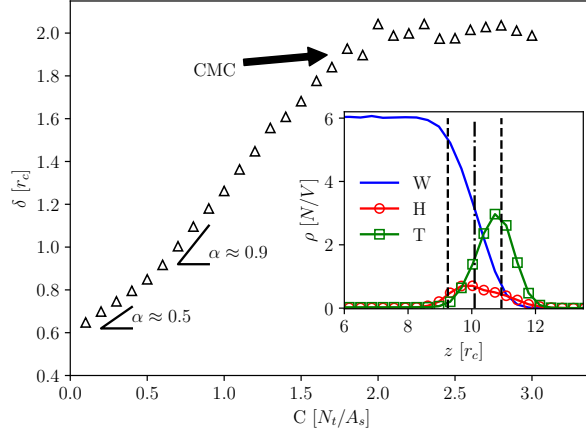


FIG. 4. Change in the interfacial thickness with the increase in the number of surfactant molecules per surface area (α gives the slope.). It remains at a constant value upon reaching the CMC. Inset: example of a density distribution near the interface for a simulation below CMC. The vertical lines indicate the position of the interface and its thickness from a hyperbolic tangent fit (Eq. 11). W, H, T are the liquid, head, and tail beads, respectively.

performed an additional 10^6 time steps of simulation to acquire data for calculating the properties of the system. A representative configuration of an equilibrated system is visually depicted in Figure 2. To determine the surface tension, we employed the Kirkwood–Buff method,⁴⁸ i.e.,

$$\gamma = \frac{L_z}{2} \left(P_{zz} - \frac{P_{xx} + P_{yy}}{2} \right) \quad (10)$$

where P_{zz} is the normal component of the pressure tensor, while P_{xx} and P_{yy} are the components of the tangential directions to the liquid–vapor surfaces. An equally significant parameter is the surface-excess concentration of surfactants. These compounds have a natural propensity to adsorb at the liquid interface until reaching a point of saturation, where the surface-excess concentration attains its maximum, while surface tension γ reaches its minimum. Beyond this saturation threshold, the introduction of additional surfactants leads to their aggregation within the bulk liquid, forming the micelles. In Figure 3, we present the findings that illustrate the variation of both the surface tension and the surface excess concentration in response to differing surfactant concentrations. In addition, the CMC point is clearly discernible in our results and shown in the plot.

The interfacial thickness is another important quantity in describing the region affected by surfactants along a fluid’s interface. This measurement can be obtained by fitting the density

distribution of w particles across the interface using the hyperbolic tangent function

$$\rho(z) = \frac{\rho_l}{2} \left[1 - \tanh \left(\frac{2(r - R_0)}{\delta} \right) \right] \quad (11)$$

where ρ_l represents the bulk density of the liquid phase, R_0 is the Gibbs dividing surface position and δ the thickness of the interface. An example of such a distribution is depicted in the inset plot of Fig. 4 for a simulation with $C = 1.5$. We can see how the density of w particles changes from the liquid phase where $\rho = 6.05$ to the vapor phase with $\rho \approx 0$ and the vertical lines indicate the Gibbs dividing surface (dash-dot) and the thickness of the interface (dashed). The density of each surfactant particle is also notable and it shows that the head group H tends to stay closer to the liquid phase while the tail particles are much closer to the vapor phase. The primary plot in Fig.4 showcases the variation in interfacial thickness. As surfactant concentration rises, δ increases until it reaches a plateau value when $C = 1.8$, indicating the CMC saturation point. For concentrations below 0.6, the thickness increases linearly with slope $\alpha \approx 0.5$ and between $C = 0.6$ and the CMC with slope $\alpha \approx 0.9$. These two linear regimes can be explained by the orientation of the surfactant molecules with respect to the interface. At lower concentrations, the surfactant tails stay in contact with the liquid surface, while at a higher concentration they become more packed orienting in the normal direction to the surface due to the decrease in available surface area per molecule.³⁷ In this sense, the cross-over at $C = 0.6$ reflects the range of the interactions between individual surfactant molecules at the fluid surface.

B. Wavenumber and droplet sizes

Following our previous work with pure liquid threads,³⁴ we have determined the characteristic wavelength of the breakup process, expressed by the reduced wavenumber $\chi = 2\pi R_0/\lambda$. This is done by computing the density correlation function along the z direction,⁴⁹ that is the direction along the thread. To construct our initial configuration, we first make a water cylinder with unperturbed radius $R_0 = 8$ and length $L_z = 24$, which is stable ($L_z < 2\pi R_0$) and does not break. In turn, we add the surfactant molecules on its surface, according to the desired concentration and we run the system for 2×10^5 time steps to reach equilibrium. After reaching equilibrium, we replicate the system in the z direction 48 times to obtain a long thread and let it evolve in time until it breaks up and all droplets are formed. We have already verified that possible finite-size effects in the direction along the thread quickly disappear, but long threads enable a more accurate calculation

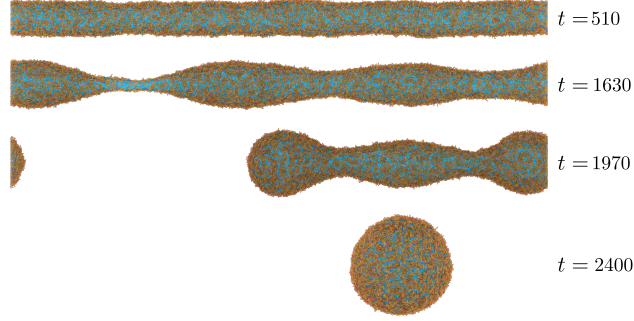


FIG. 5. Simulation snapshots of the breakup process of a small liquid thread. The system develops perturbations that grow with time and lead to the pinch-off and subsequent formation of a droplet. The concentration of surfactants is below CMC in this example. The threads used for statistical analysis were four times longer in the axial direction than the simulation shown here, which was shortened for the sake of clarity.

of the characteristic length scale of the breakup process when realizing the Fourier transform of the density–density correlation, as has already been shown for pure liquid droplets.³⁴ Moreover, long threads naturally lead to the formation of a larger number of droplets, which in turn allows for better statistics on the properties of the main and satellite droplets. We realized 20 such simulations for each surfactant concentration and the averaged results are discussed in this study. A time sequence of snapshots that leads to the formation of a single droplet is presented in Figure 5. In this example, a shorter thread simulation is being shown just for clarity as the longer threads would be poorly represented on a plot due to its dimensions. To form this thread, we replicate the equilibrated system 12 times in the axial direction, giving thread length $L = 12L_z$. It is clearly visible that a perturbation starts to develop with $\lambda \approx L/3$, but, due to asynchronous breakup, only one final droplet is formed, a mechanism that has been explained in detail in our previous work with pure liquids.³⁴

As indicated by our results, increasing surfactant concentration leads to a notable reduction in the surface tension. Since surface tension acts as the primary force of the instability, its decrease subsequently decelerates the overall breakup process. This is visually evident in Figure 6, showcasing a discernible growth in the time required for the thread to break ($t_{break-up}$), which shows a linear growth with surfactant concentration, also beyond the CMC. Moreover, the characteristic wavenumber, χ (see Ref. 34 for details on calculating χ), decreases as more surfactant is added to the system, which means that perturbations with longer wavelengths become more effective in

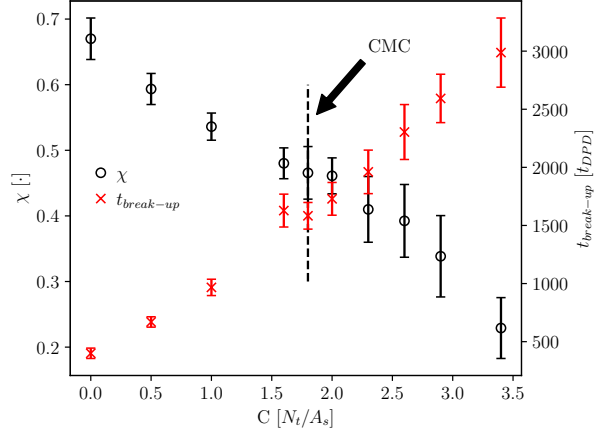


FIG. 6. Change in reduced characteristic wavenumber and time to breakup vs total surfactant concentration (total number of surfactant molecules divided by the initial surface area of the system).

destabilizing the liquid thread. However, this decrease is not only due to the change in surface tension caused by the surfactants as γ remains constant for concentrations above the CMC. Thus, the formation of micelles also adds viscous effects in the liquid bulk which explains the further slow-down of the breakup process above CMC. We also observe an increase in the standard deviation in our measurements, which can be attributed to the increase of the thermocapillary length consequently intensifying the significance of fluctuations within the system.

After the breakup, we track the number of main and satellite droplets over time by doing a cluster analysis with the software OVITO.⁵⁰ The clusters were defined as a group of particles that are close to each other within a threshold value and the droplet sizes were obtained from the radius of gyration of spherical clusters following the protocols of our previous work.³⁴ Figure 7 shows the increase in size of the main droplets formed as surfactant concentration increases. This change in size is expected as the wavelengths that lead to the breakup also increase, subsequently forming fewer pinching points along the thread axis. There is a slight difference between systems below and above CMC in how the main droplet sizes increase. This can be explained by the slowing down of the breakup process, which favors the suppression of pinching in a few regions of the thread, similar to what is depicted in Figure 5. Furthermore, we could not observe any statistically significant variation in the satellite droplet size with concentration, it having values in the range $R_s/R_0 = 0.24 \pm 0.03$ in all the simulated cases. However, there is a clear reduction in the proportion in which they are formed as C increases that could also be attributed to the larger thermocapillary

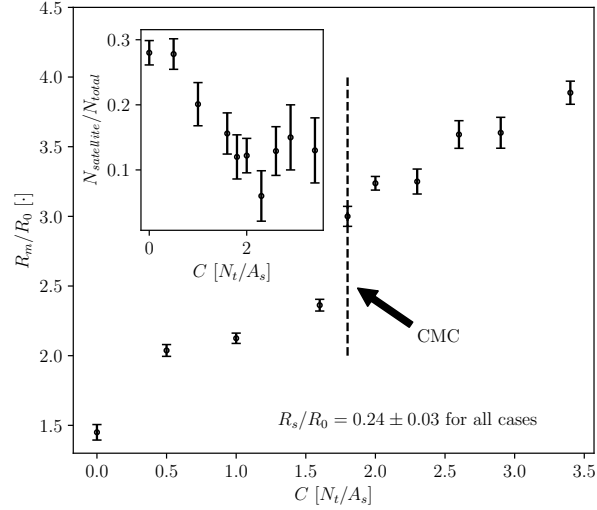


FIG. 7. Size of main droplets R_m normalized with the initial thread radius vs total surfactant concentration, C . The radius of satellite droplets did not present any statistically significant variation with respect to the change in concentration, and therefore data are now plotted here (see main text for further details). Inset shows the change in the proportion between the number of satellite droplets and the total number of droplets formed.

length scale, since thermal fluctuations are believed to inhibit their formation.¹ This proportion approximately attains an asymptotic value above CAC as shown in the inset of Figure 7.

C. Surfactant distribution at the liquid–vapor interface

Since the breakup is influenced by surface tension, describing how the surfactant is distributed along the interface is of great importance in understanding the pinch-off process and the formation of droplets. To capture these distributions, we investigated two systems below and two above the CMC, conducting 20 simulations for each system. These simulations were done with short liquid threads where $L_z = \lambda_c = 2\pi R_0/\chi$, ensuring breakup driven by the most unstable perturbation. Utilizing OVITO software,⁵⁰ we separated the particles into axial bins and tracked interface particles. Circles were fitted to these particles' positions in each bin, with their radii defining the interface profile h . Additionally, surfactant molecules within each bin were quantified, and assigned to the surface if within an interface thickness δ from h or otherwise to the bulk phase. The number of molecules on the surface N_s and in the bulk N_b are divided by the surface area A on each bin to obtain the surface excess Γ and the bulk concentration C_b .

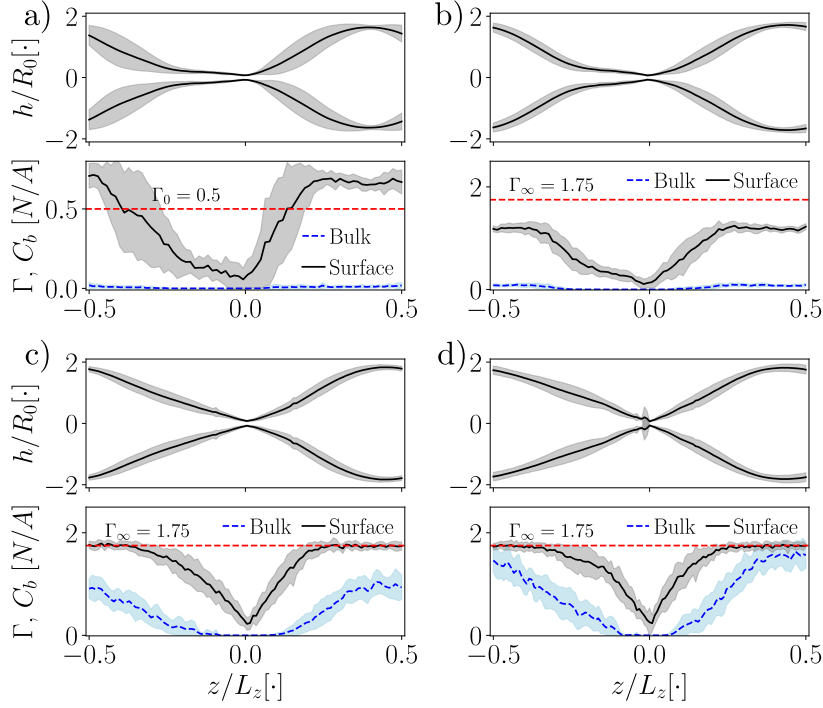


FIG. 8. Profile shapes, h/R_0 , and surfactant concentration along the z axis at the surface and in the bulk of the fluid. Lines represent the ensemble average and shaded area is one standard deviation. The averages were obtained at the moment of pinch-off and for two surfactant concentrations below CMC, a) $C = 0.5$ and b) $C = 1.0$, and two above CMC, c) $C = 2.3$ and d) $C = 2.9$. Γ_∞ is the highest surfactant excess concentration at surface saturation. Γ is the surface excess concentration and C_b is the bulk concentration (number of molecules per surface area).

Figure 8 shows the breakup profile near the pinch-off of all the studied cases and the surfactant concentration distribution on the surface and in the bulk phases. Because of the stochastic nature of the breakup, the averages were taken by shifting the pinching point to $z = 0$ and by flipping the profiles whenever $\int_{-L/2}^0 hdz > \int_0^{L/2} hdz$ to preserve large anti-symmetrical effects.³² The lines show the ensemble-averaged profile and the shaded area is within one standard deviation. In the instance of the lowest surfactant concentration, a prolonged neck emerges between droplets with an asymmetrical pinching point, deviating from the symmetrical double-cone profile predicted for thermal fluctuation breakup. As surfactant concentration increases, an asymmetrical double cone profile begins to manifest, becoming almost symmetrical for the highest concentration.

The different panels of Fig. 8 illustrate the distribution patterns of surfactant molecules within both the surface and bulk regions along the axis of the liquid thread. In the scenario where the initial concentration is at its lowest (panel a), an expected absence of surfactant molecules in the bulk phase is observed. This absence is attributed to the distance from the CMC. Furthermore, a discernible advection of surfactants is witnessed, characterized by a reduction in surface concentration around the pinching point and a subsequent increase beyond its initial value of $\Gamma = 0.5$ within the region occupied by the primary droplet. Contrary to this case, in all other instances, the presence of molecules within the bulk phase is evident. Both surface and bulk surfactants exhibit an advective motion away from the pinching point. In addition, it is noteworthy that the surface concentration consistently remains below the saturation concentration Γ_∞ . An analysis of the temporal evolution, specifically examining the case with the highest initial concentration as illustrated in Fig. 9, indicates a trajectory wherein the advected surface surfactants migrate toward the main droplet region and subsequently infiltrate the bulk phase. This observation suggests a directional flow pattern, wherein surfactant molecules, once advected from the surface around the pinching point, are transported towards the primary droplet region and eventually integrate into the bulk phase.

D. Neck-radius scaling

Thinning dynamics of liquid threads under varying surfactant concentrations were systematically examined by tracking the minimum neck radius h_{min} until the pinch-off event. Four distinct cases, encompassing two surfactant concentrations below the CMC and two above, were investigated. For each case, 20 simulations were conducted, and the averaged neck radius values were obtained with respect to their relative time from the breakup (t_b) $\tau = (t_b - t)$ as presented in Fig. 10. According to a theoretical analysis of surfactant-laden breakup at the limit when surfactants are advected away from the pinching point, the minimum radius should follow the viscous regime with linear scaling $h_{min} \sim \tau$.¹⁹ However, we did not observe this scaling and at the lowest surfactant concentration, the thinning process appears to be close to the inertial regime, indicated by the scaling $h_{min} \sim \tau^{2/3}$. Interestingly, for low concentration we did not observe a clear transition or the presence of the thermal fluctuation regime $h_{min} \sim \tau^{0.418}$.²² MDPD simulations of a liquid without surfactants also have shown a deviation from the thermal fluctuation scaling.³³

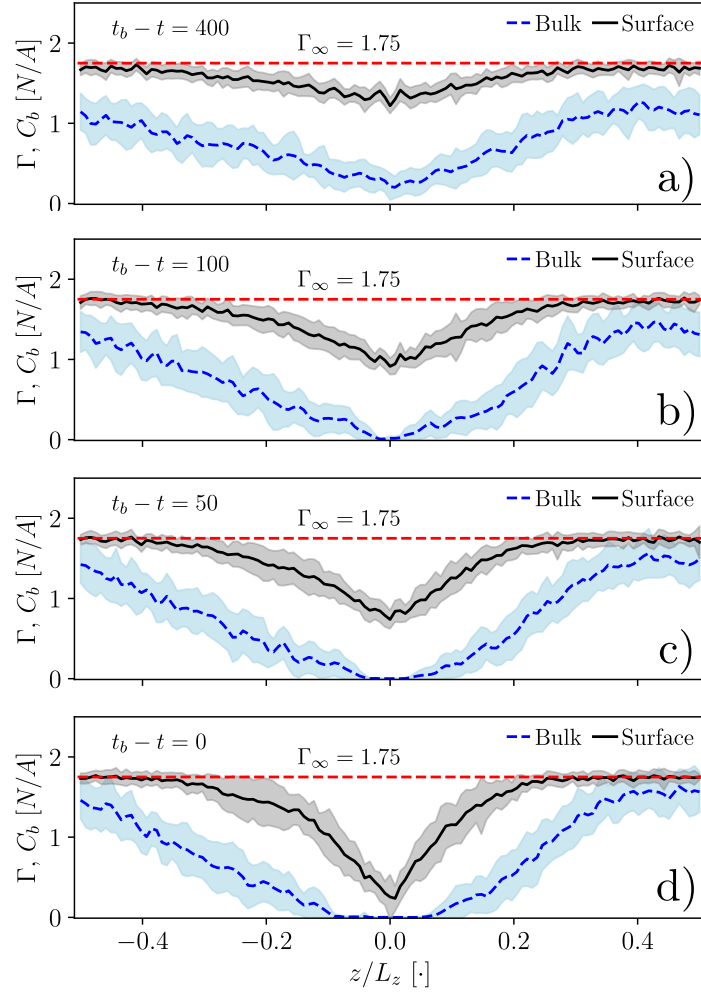


FIG. 9. Time evolution of the surfactant distribution for a case above CMC ($C = 2.9$) showing the advection of surfactants from the pinching point and increase in bulk surfactant in the main droplet region. Γ is the surface excess concentration and C_b is the bulk concentration (number of molecules per surface area). Each panel corresponds to a different point in time before the breakup moment ($t = t_b$), i.e. a) $t_b - t = 400$, b) $t_b - t = 100$, c) $t_b - t = 50$, and d) $t_b - t = 0$, as indicated.

As we increase surfactant concentration, consequently reducing surface tension, the breakup dynamics still exhibits a power-law behavior. However, the observed exponent deviates from the inertial regime and approaches the thermal fluctuation one. These results substantiate the conclusions drawn by Zhao et al.,³² who demonstrated that the scaling exponent converges towards 0.418 when the surface tension $\gamma \rightarrow 0$ from simulations using the 1D SLE model. In all of our simulations cases, we can observe a transition between the power-law to a different regime im-

mediately preceding the pinch-off event. This last regime has been proposed by Zhao et al.⁵¹ as the “breakup” regime, following a power-law with exponent 0. However, no further explanation was given as to the physical meaning and origin of this behavior. Moreover, they only analyzed the evolution of a single simulation trajectory instead of an ensemble average. From our results, the transition actually occurs when h_{min} reaches below the cutoff radius of the particle interactions and it could be an artifact from the MDPD method. When the thread reaches such scales, the local density $\bar{\rho}$ (see Eq. 5) starts to decrease with time and this, in turn, reduces the strength of the repulsive term in the conservative force, leading to a stronger relative attraction between the particles that slows down the thinning process. This possible regime scales not as power-law but seemingly as $h_{min} \sim e^{\tau}$. Exponential thinning is also found in the breakup of viscoelastic fluids²¹ and when surface rheological effects are taken into account.^{20,52}

IV. CONCLUSIONS

In this study, we investigated the impact of surfactants on the breakup of a liquid thread under thermal fluctuations by employing simulations via the particle-based mesoscale method MDPD. We characterized the HT3 coarse-grained surfactant model in terms of its relevant interfacial properties such as surface tension and interface thickness. Furthermore, the model also features the spontaneous formation of micelles above the CMC. The results indicate that the model is adequate in reproducing the behavior of real surfactant molecules. Then, a detailed study of the breakup of liquid threads in the presence of surfactant was carried out. We find that increased surfactant concentration would naturally lead to the increase in the most unstable wavelength that characterizes the breakup, and, also, in the time for it to occur. At first, this could be explained by the decrease in surface tension which, in turn, increases the Oh number. However, both the wavelength and time to breakup keep increasing for concentrations above the CMC, where surface tension remains constant. This might therefore be due to bulk viscous effects from the increase in surfactant micelle concentration. We also discussed the minimum radius scaling of the thinning process and showed that the observed power-law behavior matches the I regime and approaches the TF regime, depending on the surfactant concentration — low and high, respectively. At low concentrations, we found that the breakup is in the I regime instead of the universal VI or V regimes. Nonetheless, this result is in agreement with experimental measurements.⁵³ At higher concentrations, the thinning dynamics transition into the thermal fluctuation regime. Moreover, we argue that the “breakup”

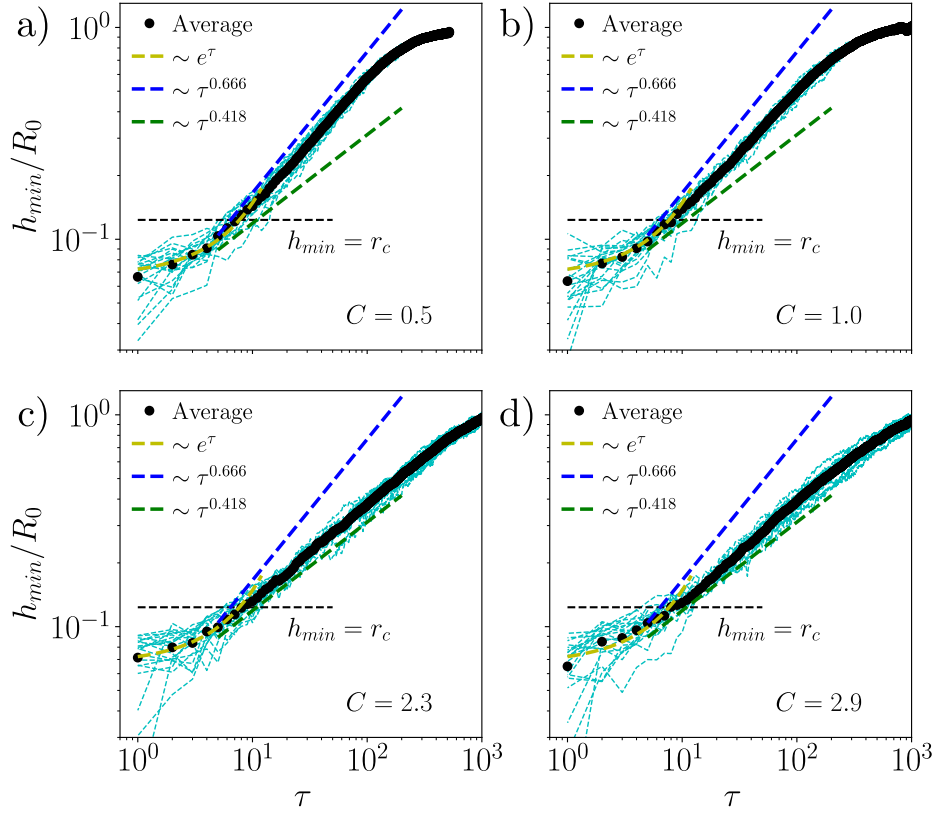


FIG. 10. Radius scaling of the thinning process for threads with four different surfactant concentrations and comparison with known breakup regimes. a) $C = 0.5$; b) $C = 1.6$; c) $C = 2.3$; d) $C = 2.9$. Each case is an ensemble average of 20 simulations. r_c is the cutoff distance for the attractive interaction. Dashed lines were added just as reference to the theoretical regimes and have the same values in all plots.

thinning regime proposed by Zhao et al.³² might be an artifact of the MDPD model as the transition into it occurs when h_{min} approaches the cutoff of the interactions. When the minimum radius is below the cutoff, the attraction between particles becomes increasingly more dominant than the repulsion leading to the slow-down of the thinning dynamics. Finally, we have examined the breakup profiles and surfactant distribution of the threads providing molecular-level insights into the mechanisms of this phenomenon. Thus, we anticipate that our study sheds light on the thus far poorly investigated breakup of liquid threads laden with surfactant.

ACKNOWLEDGMENTS

This research has been supported by the National Science Centre, Poland, under grant No. 2019/34/E/ST3/00232. We gratefully acknowledge Polish high-performance computing infrastructure PLGrid (HPC Centers: ACK Cyfronet AGH) for providing computer facilities and support within computational grant no. PLG/2022/015747.

REFERENCES

- ¹M. Moseler and U. Landman, “Formation, stability and breakup of nanojets,” *Science* **289**, 1165–1169 (2000).
- ²O. A. Basaran, H. Gao, and P. P. Bhat, “Nonstandard inkjets,” *Ann. Rev. Fluid Mech.* **45**, 85–113 (2013).
- ³Y. Y. Ye, R. Biswas, J. R. Morris, A. Bastawros, and A. Chandra, “Molecular dynamics simulation of nanoscale machining of copper,” *Nanotechnology* **14**, 390–396 (2003).
- ⁴H. Wu, F. Zhang, and Z. Zhang, “Droplet breakup and coalescence of an internal-mixing twin-fluid spray,” *Phys. Fluids* **33**, 013317 (2021).
- ⁵S. D. Hoath, *Fundamentals of Inkjet Printing: The Science of Inkjet and Droplets* (John Wiley & Sons, Cambridge, 2016).
- ⁶S. M. Mousavi, D. Jarrahbashi, B. J. Lee, N. Karimi, and S. A. Faroughi, “Impact of hybrid surfaces on the droplet breakup dynamics in microgravity slug flow: A dynamic contact angle analysis,” *Phys. Fluids* **35**, 072003 (2023).
- ⁷S. M. Mousavi and B. J. Lee, “Investigation of bubble structure in a microchannel under microgravity conditions: Effects of discontinuous wettability with dynamic contact angle,” *Acta Astronaut.* **201**, 394–400 (2022).
- ⁸S. M. Mousavi, F. Sotoudeh, B. J. Lee, M.-R. Paydari, and N. Karimi, “Effect of hybrid wall contact angles on slug flow behavior in a t-junction microchannel: A numerical study,” *Colloids Surf. A: Physicochem. Eng. Asp.* **650**, 129677 (2022).
- ⁹S. Heydarpoor and N. M. Famili, “Polygon model for solution of non-linear velocity gradient of interface and asymmetric break-up of droplet,” *Phys. Fluids* **36**, 012103 (2024).

- ¹⁰S. Zhao, Z. Liu, N. Zheng, C. Zhang, F. Cai, K. Zheng, and Y. Pang, “Formation characteristics and acoustic regulation of liquid metal droplets in low-aspect-ratio channels,” *Phys. Fluids* **36**, 012017 (2024).
- ¹¹J. Plateau, “Experimental and theoretical researches on the figures of equilibrium of a liquid mass withdrawn from the action of gravity,” *Philos. Mag., Ser. 4* **14**, 431–451 (1857).
- ¹²L. Rayleigh, “On the instability of jets,” *Proc. London Math. Soc.* **s1-10**, 4–13 (1878).
- ¹³C. Weber, “Zum zerfalleines flüssigkeitsstrahles,” *J. Appl. Math. Mech.* **11**, 136–154 (1931).
- ¹⁴F. Goodarzi and S. Zendejboudi, “A comprehensive review on emulsions and emulsion stability in chemical and energy industries,” *Can. J. Chem. Eng.* **97**, 281–309 (2019).
- ¹⁵N. M. Kovalchuk, H. Jenkinson, R. Miller, and M. J. Simmons, “Effect of soluble surfactants on pinch-off of moderately viscous drops and satellite size,” *J. Colloid Interface Sci.* **516**, 182–191 (2018).
- ¹⁶J. Eggers, “Universal pinching of 3D axisymmetric free-surface flow,” *Phys. Rev. Lett.* **71**, 3458–3460 (1993).
- ¹⁷D. T. Papageorgiou, “On the breakup of viscous liquid threads,” *Phys. Fluids* **7**, 1529–1544 (1995).
- ¹⁸J. R. Castrejón-Pita, A. A. Castrejón-Pita, S. S. Thete, K. Sambath, I. M. Hutchings, J. Hinch, J. R. Lister, and O. A. Basaran, “Plethora of transitions during breakup of liquid filaments,” *Proc. Natl. Acad. Sci. U.S.A.* **112**, 4582–4587 (2015).
- ¹⁹H. Wee, B. W. Wagoner, P. M. Kamat, and O. A. Basaran, “Effects of Surface Viscosity on Breakup of Viscous Threads,” *Phys. Rev. Lett.* **124**, 204501 (2020).
- ²⁰A. Martínez-Calvo and A. Sevilla, “Universal Thinning of Liquid Filaments under Dominant Surface Forces,” *Phys. Rev. Lett.* **125**, 114502 (2020).
- ²¹H.-C. Chang, E. A. Demekhin, and E. Kalaidin, “Iterated stretching of viscoelastic jets,” *Phys. Fluids* **11**, 1717–1737 (1999).
- ²²J. Eggers, “Dynamics of Liquid Nanojets,” *Phys. Rev. Lett.* **89**, 084502 (2002).
- ²³Y. Hennequin, D. G. A. L. Aarts, J. H. van der Wiel, G. Wegdam, J. Eggers, H. N. W. Lekkerkerker, and D. Bonn, “Drop formation by thermal fluctuations at an ultralow surface tension,” *Phys. Rev. Lett.* **97**, 244502 (2006).
- ²⁴J. Petit, D. Rivi re, H. Kellay, and J. P. Delville, “Break-up dynamics of fluctuating liquid threads,” *Proc. Natl. Acad. Sci. U.S.A.* **109**, 18327–18331 (2012).
- ²⁵I. Pagonabarraga and D. Frenkel, “Non-Ideal DPD Fluids,” *Mol. Simul.* **25**, 167–175 (2000).

- ²⁶I. Pagonabarraga and D. Frenkel, “Dissipative particle dynamics for interacting systems,” *J. Chem. Phys.* **115**, 5015–5026 (2001).
- ²⁷P. B. Warren, “Vapor-liquid coexistence in many-body dissipative particle dynamics,” *Phys. Rev. E* **68**, 066702 (2003).
- ²⁸A. Tiwari and J. Abraham, “Dissipative particle dynamics simulations of liquid nanojet breakup,” *Microfluid. Nanofluidics* **4**, 227–235 (2008).
- ²⁹A. Tiwari, H. Reddy, S. Mukhopadhyay, and J. Abraham, “Simulations of liquid nanocylinder breakup with dissipative particle dynamics,” *Phys. Rev. E* **78**, 016305 (2008).
- ³⁰C.-j. Mo, L.-j. Yang, F. Zhao, and K.-d. Cui, “Mesoscopic simulation of a thinning liquid bridge using the dissipative particle dynamics method,” *Phys. Rev. E* **92**, 023008 (2015).
- ³¹M. Arienti, W. Pan, X. Li, and G. Karniadakis, “Many-body dissipative particle dynamics simulation of liquid/vapor and liquid/solid interactions,” *J. Chem. Phys.* **134**, 204114 (2011).
- ³²C. Zhao, D. A. Lockerby, and J. E. Sprittles, “Dynamics of liquid nanothreads: Fluctuation-driven instability and rupture,” *Phys. Rev. Fluids* **5**, 044201 (2020).
- ³³C. Zhao, J. Zhao, T. Si, and S. Chen, “Influence of thermal fluctuations on nanoscale free-surface flows: A many-body dissipative particle dynamics study,” *Phys. Fluids* **33**, 112004 (2021).
- ³⁴L. H. Carnevale, P. Deuar, Z. Che, and P. E. Theodorakis, “Liquid thread breakup and the formation of satellite droplets,” *Phys. Fluids* **35**, 074108 (2023).
- ³⁵A. Ghoufi, J. Emile, and P. Malfreyt, “Recent advances in Many Body Dissipative Particles Dynamics simulations of liquid-vapor interfaces,” *Europ. Phys. J. E* **36**, 10 (2013).
- ³⁶P. Zhou, J. Hou, Y. Yan, J. Wang, and W. Chen, “Effect of Aggregation and Adsorption Behavior on the Flow Resistance of Surfactant Fluid on Smooth and Rough Surfaces: A Many-Body Dissipative Particle Dynamics Study,” *Langmuir* **35**, 8110–8120 (2019).
- ³⁷R. L. Hendrikse, C. Amador, and M. R. Wilson, “A many-body dissipative particle dynamics parametrisation scheme to study behaviour at air–water interfaces,” *Soft Matter* **19**, 3590–3604 (2023).
- ³⁸P. J. Hoogerbrugge and J. M. V. A. Koelman, “Simulating Microscopic Hydrodynamic Phenomena with Dissipative Particle Dynamics,” *Europhys. Lett. (EPL)* **19**, 155–160 (1992).
- ³⁹E. Lavagnini, J. L. Cook, P. B. Warren, and C. A. Hunter, “Translation of chemical structure into dissipative particle dynamics parameters for simulation of surfactant self-assembly,” *J. Phys. Chem. B* **125**, 3942–3952 (2021).

- ⁴⁰R. D. Groot and P. B. Warren, “Dissipative particle dynamics: Bridging the gap between atomistic and mesoscopic simulation,” *J. Chem. Phys.* **107**, 4423–4435 (1997).
- ⁴¹P. Vanya, P. Crout, J. Sharman, and J. A. Elliott, “Liquid-phase parametrization and solidification in many-body dissipative particle dynamics,” *Phys. Rev. E* **98**, 033310 (2018).
- ⁴²Z.-B. Wang, R. Chen, H. Wang, Q. Liao, X. Zhu, and S.-Z. Li, “An overview of smoothed particle hydrodynamics for simulating multiphase flow,” *Appl. Math. Model.* **40**, 9625–9655 (2016).
- ⁴³P. Español and P. Warren, “Statistical Mechanics of Dissipative Particle Dynamics,” *Europhys. Lett. (EPL)* **30**, 191–196 (1995).
- ⁴⁴P. B. Warren, “No-go theorem in many-body dissipative particle dynamics,” *Phys. Rev. E* **87**, 045303 (2013).
- ⁴⁵P. Vanya and J. A. Elliott, “Definitions of local density in density-dependent potentials for mixtures,” *Phys. Rev. E* **102**, 013312 (2020).
- ⁴⁶A. Ghoufi and P. Malfreyt, “Mesoscale modeling of the water liquid-vapor interface: A surface tension calculation,” *Phys. Rev. E* **83**, 051601 (2011).
- ⁴⁷Y. Zhu, X. Bai, and G. Hu, “Interfacial behavior of phospholipid monolayers revealed by mesoscopic simulation,” *Biophys. J.* **120**, 4751–4762 (2021).
- ⁴⁸J. G. Kirkwood and F. P. Buff, “The Statistical Mechanical Theory of Surface Tension,” *J. Chem. Phys.* **17**, 338–343 (1949).
- ⁴⁹P. E. Theodorakis, W. Paul, and K. Binder, “Microphase separation in bottlebrush polymers under poor-solvent conditions,” *EPL (Europhys. Lett.)* **88**, 63002 (2009).
- ⁵⁰A. Stukowski, “Visualization and analysis of atomistic simulation data with ovito—the open visualization tool,” *Modelling Simul. Mater. Sci. Eng.* **18**, 015012 (2010).
- ⁵¹J. Zhao, N. Zhou, K. Zhang, S. Chen, Y. Liu, and Y. Wang, “Rupture process of liquid bridges: The effects of thermal fluctuations,” *Phys. Rev. E* **102**, 023116 (2020).
- ⁵²H. Wee, B. W. Wagoner, and O. A. Basaran, “Absence of scaling transitions in breakup of liquid jets caused by surface viscosity,” *Phys. Rev. Fluids* **7**, 074001 (2022).
- ⁵³N. M. Kovalchuk, E. Nowak, and M. J. H. Simmons, “Effect of Soluble Surfactants on the Kinetics of Thinning of Liquid Bridges during Drops Formation and on Size of Satellite Droplets,” *Langmuir* **32**, 5069–5077 (2016).